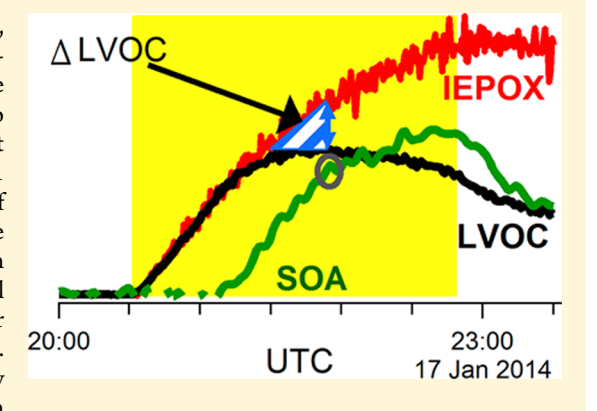


Formation of Low Volatility Organic Compounds and Secondary Organic Aerosol from Isoprene Hydroxyhydroperoxide Low-NO Oxidation

Jordan E. Krechmer,^{†,‡} Matthew M. Coggon,[§] Paola Massoli,[∥] Tran B. Nguyen,^{§,⊥} John D. Crounse, [⊥] Weiwei Hu,^{†,‡} Douglas A. Day,^{†,‡} Geoffrey S. Tyndall,[#] Daven K. Henze, [▽] Jean C. Rivera-Rios,^{○,%} John B. Nowak, [∥] Joel R. Kimmel, ^{∥,♠} Roy L. Mauldin, III, [¶] Harald Stark, ^{†,‡,∥} John T. Jayne, [∥] Mikko Sipilä, [∞] Heikki Junninen, [∞] Jason M. St. Clair, ^{⊥,∫} Xuan Zhang, [§] Philip A. Feiner, [★] Li Zhang, [★] David O. Miller, [★] William H. Brune, [★] Frank N. Keutsch, ^{○,%} Paul O. Wennberg, [⊥] John H. Seinfeld, ^{§,♠} Douglas R. Worsnop, [∥] Jose L. Jimenez, ^{*,†,‡} and Manjula R. Canagaratna ^{*,∥}

Supporting Information

ABSTRACT: Gas-phase low volatility organic compounds (LVOC), produced from oxidation of isoprene 4-hydroxy-3-hydroperoxide (4,3-ISOPOOH) under low-NO conditions, were observed during the FIXCIT chamber study. Decreases in LVOC directly correspond to appearance and growth in secondary organic aerosol (SOA) of consistent elemental composition, indicating that LVOC condense (at OA below 1 μg m⁻³). This represents the first simultaneous measurement of condensing low volatility species from isoprene oxidation in both the gas and particle phases. The SOA formation in this study is separate from previously described isoprene epoxydiol (IEPOX) uptake. Assigning all condensing LVOC signals to 4,3-ISOPOOH oxidation in the chamber study implies a wall-loss corrected non-IEPOX SOA mass yield of ~4%. By contrast to monoterpene oxidation, in which extremely low volatility VOC (ELVOC) constitute the organic aerosol, in the isoprene system



LVOC with saturation concentrations from 10^{-2} to $10 \mu g m^{-3}$ are the main constituents. These LVOC may be important for the growth of nanoparticles in environments with low OA concentrations. LVOC observed in the chamber were also observed in the atmosphere during SOAS-2013 in the Southeastern United States, with the expected diurnal cycle. This previously uncharacterized aerosol formation pathway could account for ~5.0 Tg yr⁻¹ of SOA production, or 3.3% of global SOA.

INTRODUCTION

Atmospheric aerosols can have detrimental effects on human health¹ and are known to affect global climate both directly and indirectly.² Secondary Organic Aerosol (SOA) forms in the Received: April 23, 2015 July 17, 2015 Revised: Accepted: July 24, 2015 Published: July 24, 2015

[†]Cooperative Institute for Research in Environmental Sciences (CIRES), Boulder, Colorado 80309, United States

[‡]Department of Chemistry and Biochemistry, University of Colorado, Boulder, Colorado 80309, United States

[§]Divisions of Chemistry and Chemical Engineering, California Institute of Technology, Pasadena, California 91125, United States

Center for Aerosol and Cloud Chemistry, Aerodyne Research, Billerica, Massachusetts 01821, United States

¹Division of Geological and Planetary Sciences, California Institute of Technology, Pasadena, California 91125, United States

^{*}National Center for Atmospheric Research, Boulder, Colorado 80301, United States

^VDepartment of Mechanical Engineering, University of Colorado, Boulder, Colorado 80309, United States

Operatment of Chemistry, University of Wisconsin-Madison, Madison, Wisconsin 53706, United States

[◆]Tofwerk, AG, CH-3600, Thun, Switzerland

[¶]Department of Atmospheric and Oceanic Sciences, University of Colorado, Boulder, Colorado 80309, United States

[∞]Department of Physics, University of Helsinki, 00014, Helsinki, Finland

^{*}Department of Meteorology, Pennsylvania State University, University Park, Pennsylvania 16802, United States

Division of Engineering and Applied Science, California Institute of Technology, Pasadena, California 91125, United States

atmosphere by the oxidation of volatile organic compounds (VOCs), and typically is a major fraction of submicron aerosol mass.^{3,4} VOCs can be emitted by human activity (anthropogenic) or vegetation (biogenic). While significant progress has been made in identifying VOC precursors and formation pathways of SOA, there is still significant uncertainty in these chemical processes and in the SOA global budget.^{4–6}

Isoprene is a biogenic VOC and represents the largest emission of nonmethane hydrocarbons to the Earth's atmosphere with global emissions of ~535 Tg C yr^{-1,7,8} In the atmosphere, isoprene reacts readily with hydroxyl radicals (OH) to produce organic peroxyl radicals (RO₂) that, under low-NO conditions, subsequently react with hydroperoxyl radicals (HO₂) and form isoprene hydroxyhydroperoxides (ISOPOOH, C₅H₁₀O₃).^{9,10} Of the ISOPOOH isomers, two are atmospherically important: 4,3-ISOPOOH and 1,2-ISOPOOH. 11 The further oxidation of ISOPOOH by OH produces key isoprene low-NO SOA precursor intermediates, isoprene epoxydiols (IEPOX, C₅H₁₀O₃), at yields greater than 75%. 10,12 Isoprene has been shown to form SOA under a variety of atmospheric conditions through various chemical pathways, including the heterogeneous uptake of IEPOX onto wet sulfate aerosol. 10,13-17 With reported SOA yields from isoprene that range from 1-6% (although these may be lower limits) 18,19 biogenic emissions are thought to dominate the global sources of SOA with isoprene accounting for a substantial fraction.²⁰

To date, most biogenic SOA formation and evolution mechanisms include equilibrium partitioning between semivolatile gas-phase compounds (SVOC) and a liquid organic particle phase. 21,22 Recently Ehn et al. reported a new source of SOA from the irreversible condensation of extremely lowvolatility organic compounds (ELVOC) produced from the ozonolysis of monoterpenes both in laboratory studies and ambient conditions.^{23*} In the laboratory, ELVOC were produced on rapid time scales from α -pinene, β -pinene, limonene, and cyclohexene and irreversibly condensed onto seed aerosol. High molar yields were observed: 7% for α -pinene and 17% for limonene. Detailed follow-up studies suggest that this process results from a peroxy radical (RO₂) autoxidation mechanism,²⁴ similar to that proposed by Crounse et al.²⁵ Compared to SVOC, the extremely low volatility of ELVOC makes their relative contribution to SOA yields larger at low OA loadings, and makes them relevant to the growth of nanoparticles.

In this work, we directly investigate, using simultaneous gasphase and particle composition measurements obtained during a chamber experiment, the link between low volatility organic compounds (LVOC) and SOA generated from the photo-oxidation of ISOPOOH and associated species under low NO conditions. We use a kinetic box model to investigate this production pathway, and present ambient measurements from the recent Southern Oxidant and Aerosol Study (SOAS; June—July 2013; http://soas2013.rutgers.edu/) to illustrate the impact of this pathway under ambient conditions. The properties of the identified condensing gas-phase species and the potential importance of this pathway for SOA formation from isoprene are discussed.

■ EXPERIMENTAL SECTION

Atmospheric Chamber Experiments. Chamber experiments were performed as part of the Focused Isoprene experiment at the California Institute of Technology (FIXCIT)

laboratory campaign during January 2014. FIXCIT was designed to be complementary to SOAS with the goal of elucidating the mechanisms behind key ambient observations of biogenic VOC chemistry in the southeast U.S. The laboratory effort involved an array of state-of-the-art instrumentation, with 18 gas- and aerosol-phase instruments operating throughout the study. Experiments were performed in two 24 m³ FEP Teflon bags housed in an $8 \times 5 \times 3$ m insulated enclosure. A detailed description of the Caltech chamber facilities, the entire set of FIXCIT experiments, instrumentation and methods is provided in the campaign overview publication. ²⁶

This study focuses on FIXCIT experiment no. 17 (17 January 2014), which explored the OH-initiated oxidation of isoprene 4-hydroxy-3-hydroperoxy (4,3-ISOPOOH). 4,3-ISO-POOH is one of the two main atmospherically important ISOPOOH isomers (1,2-ISOPOOH is the other). 11 Approximately 54 ppb of synthesized 4,3-ISOPOOH was injected into the chamber and oxidized with a steady-state concentration of 1.2×10^6 molecules cm⁻³ of OH generated from the photolysis of 750 ppb hydrogen peroxide (H₂O₂) by UV black lights (peak at 350 nm). After 2.5 h, ~ 42 ppb of the ISOPOOH had reacted away. Aerosol growth was observed through increases in the AMS organic mass signals but no seed aerosol was added. The UV lights were then switched off and the chamber was sampled for an additional 4 h. The reaction proceeded at 26 °C and less than 5% relative humidity (RH). The experiment was performed under "low-NO" conditions with NO concentrations of less than 25 pptv during the experiment and a NO:HO₂ ratio of <1:5.

Nitrate Chemical Ionization Mass Spectrometry (NO₃⁻-CIMS). Measurements of highly oxidized gas-phase organic species were made with an Aerodyne high-resolution time-of-flight chemical ionization mass spectrometer (HRToF-CIMS), which has been described in previous publications.^{27,28} In this work, the CIMS was equipped with an atmospheric-pressure nitrate-ion (NO₃⁻) ionization source (Airmodus, Ltd.; hereafter NO₃⁻-CIMS). Originally developed and used for the detection of gas phase sulfuric acid and methanesulfonic acid,²⁹ the NO₃⁻ ions also cluster with highly oxidized organic species at high efficiency without fragmentation.^{30,31}

Air from the chamber was drawn into the NO_3^- source at a rate of 3 SLPM through FEP tubing 2.0m long and with a 7.9 mm inner diameter. The sample flow was then diluted with 8 SLPM of clean zero air (RH < 8%) to provide ~11 SLPM of total sample flow into the NO_3^- source. A flow of 0.7 SLPM of the total 11 SLPM flow was drawn directly into the mass spectrometer from the source via a 300 μ m pinhole.

Raw negative-ion spectra were acquired at a rate of 1 Hz and subsequently averaged to 1 min. Data were analyzed using the Tofware (Tofwerk, AG and Aerodyne Research, Inc., version 2.4) toolkit developed for the IGOR Pro 6 analysis software package (Wavemetrics, Inc.). The $\mathrm{NO_3}^-$ -CIMS was operated in "V-mode" and achieved a mass resolution of \sim 4100 at m/z 212 and above and a mass accuracy of <5 ppm, which enabled assignment of elemental composition to observed mass-to-charge values. A representative high-resolution fit is shown in Figure S1.

The instrument was zeroed periodically by shutting off the flow from the chamber and drawing only clean house air for several minutes. Mass-to-charge calibrations were performed before and after every experiment and were further corrected point-by-point in data analysis using a combination of both nitrate reagent ions and previously identified Teflon-related

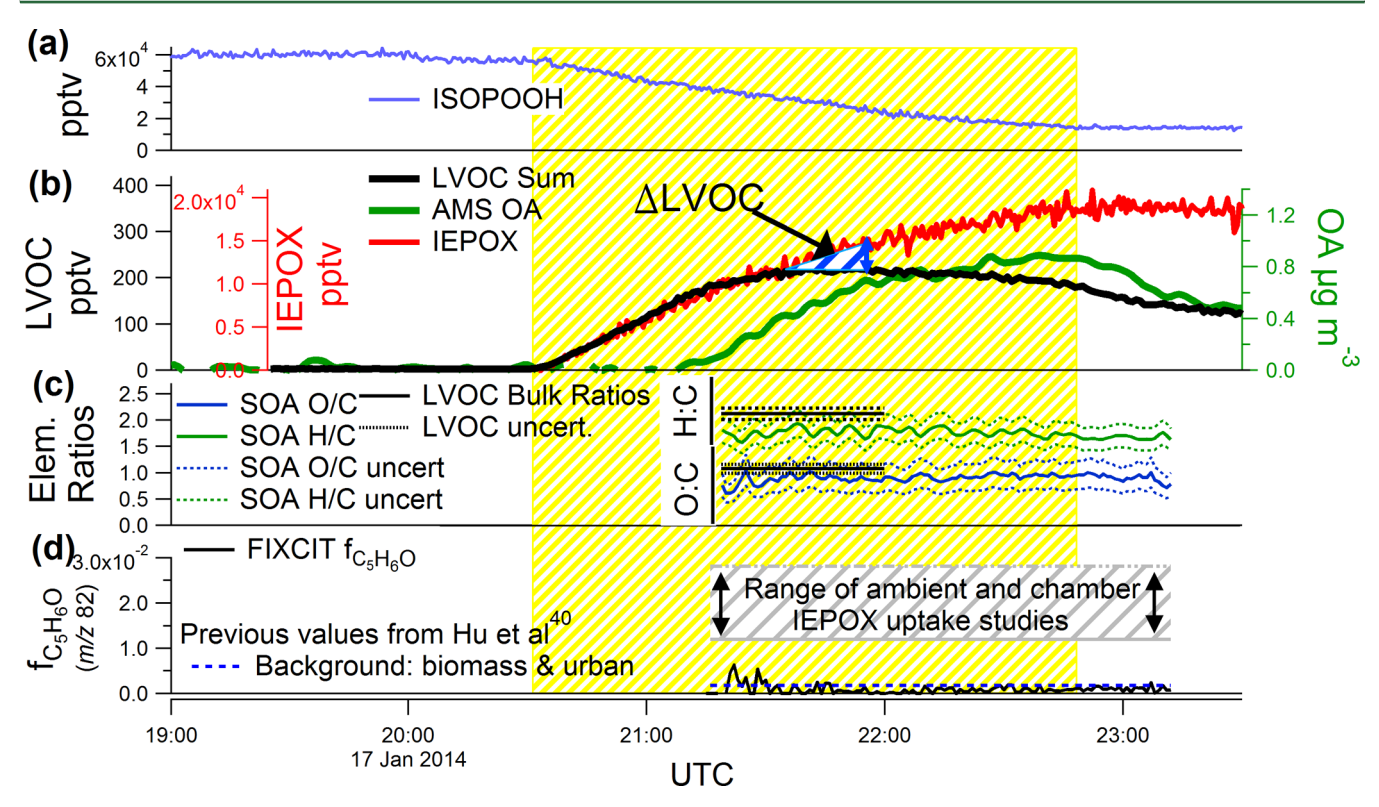


Figure 1. Figure 1. Time evolution of key species in the chamber during 4,3-ISOPOOH + OH oxidation: (a) ISOPOOH, (b) total observed LVOC, AMS SOA (with no adjustment to account for particles outside the size cutoff), and IEPOX, (c) AMS and LVOC atomic O:C and H:C, and (d) fraction of AMS signal at $C_5H_6O^+$ ($f_{C_6H_6O}$). Shaded yellow indicates UV lights on and active photochemistry.

ions coming from the inlet lines that bracket the m/z region of interest. Futher details about the NO₃--CIMS are described in the Supporting Information.

Aerosol Mass Spectrometer. Aerosol mass was measured by an Aerodyne high resolution time-of-flight aerosol mass spectrometer (hereafter AMS).³² The instrument was calibrated with 350 nm NH₄NO₃ particles, and bulk composition was analyzed using the high resolution data analysis software package PIKA. 32 Elemental analysis (EA) was performed using the recently updated parametrization by Canagaratna et al.³³

Aerosol liquid water was removed using a Nafion membrane diffusion drier prior to the AMS measurement. Aerosol losses due to particle bounce upon the AMS vaporizer were corrected using a collection efficiency (CE) of 0.75. The same CE factor was used by Nguyen et al. 14 during a study of IEPOX uptake onto ammonium sulfate seed. Line losses were observed to account for 20% of aerosol mass; accordingly, a correction factor of 1.2 was applied to all AMS data.

CF₃O⁻-CIMS. IEPOX, ISOPOOH, and other OVOC (oxygenated volatile organic compounds) measurements were obtained using CF₃O⁻-CIMS methods. 10,34,35

Compounds Associated with ISOPOOH. Other compounds (~7% by mole) present in the synthesized 4,3-ISOPOOH standard were introduced into the chamber with ISOPOOH. Two of the larger associated species initially present in the reaction chamber with potential importance to observed LVOC signals are thought to be 4,3-dihydroxy-C5alkene (~1% of ISOPOOH) and 4-hydroxy-3-keto-C5 alkene (~0.1% of ISOPOOH) (Figure S2). These compounds will react with OH at rates similar to ISOPOOH, and could have higher LVOC yields than ISOPOOH. While these species likely originated from the ISOPOOH synthesis or degradation, they

will also be produced in the atmospheric oxidation of isoprene at levels not unlike those observed in this experiment (RO₂ + RO₂ reactions being the most obvious production pathway). Here, we consider the sum of LVOC formed from all reactants present in the chamber, as there is currently insufficient information to distinguish their origin. Additional discussion on this topic is given in the Supporting Information.

Kinetic Box Model. A chemical kinetic box model (KinSim v2 for IGOR Pro; http://www.igorexchange.com/node/1333) was used to simulate key experimental observations. KinSim uses the Backward Differentiation Formula method to solve a system of chemical reactions treated as ordinary differential equations. The initial conditions were based on measured quantities and kinetic rate coefficients obtained from recent references (Table S2). Aerosol and wall uptake were calculated using measured or modeled as inputs, as appropriate, and are described in detail in the SI.

RESULTS AND DISCUSSION

Dynamics of Gas-Phase LVOC and SOA. The timedependent behavior of key species throughout the experiment is detailed in Figure 1. After the reactant concentrations stabilized following injection (Figure 1a), the UV lights were switched on at 20:30 UTC. From that point, ISOPOOH decreased due to reaction with OH and the IEPOX and LVOC concentrations increased rapidly; 45 min later, SOA was detected by the AMS and kept increasing while the LVOC concentration leveled and then decreased together with the SOA. This contrasts with the behavior of IEPOX, which continued to rise until the UV lights were turned off, at which point its concentration leveled out.

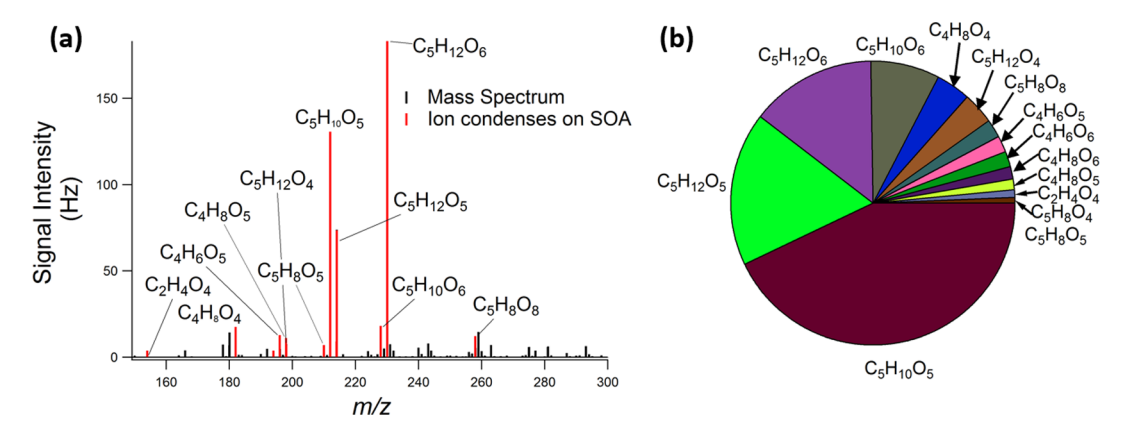


Figure 2. (a) NO₃⁻-CIMS gas-phase mass spectrum at the point of peak LVOC concentration (22:00 UTC). Species whose time evolution indicates condensation into the aerosol phase are highlighted in red. All species are detected as clusters with NO_3^- (m/z 62), which has been omitted for clarity, as have reagent ions, known contaminants, and isotopic peaks. (b) Estimated relative contributions of LVOC to the observed SOA.

We can extrapolate the slope of the initial LVOC increase to follow the time trend of IEPOX past the point where SOA appears. The difference between the extrapolated concentration and the actual LVOC trace is used as an estimate of the amount of LVOC lost to aerosol up to that point in time (Δ LVOC in Figure 1b). At 21:45 UTC, Δ LVOC was 62 pptv (0.39 μ g m⁻³) and SOA was 0.45 μ g m⁻³. The two concentrations are in good agreement within the uncertainties ($\pm 100\%$ for CIMS, $\pm 35\%$ for AMS).^{36,37} Therefore, the condensation of gas-phase LVOC from oxidation of 4,3-ISOPOOH and associated OVOC likely accounts for all or most of the SOA observed here.

FIXCIT included two other experiments (nos. 2 and 21) in which isoprene OH-initiated oxidation was investigated under low-NO conditions. Many of the same LVOC were also observed; but SOA was not detected by the AMS in those experiments. It is unlikely that the LVOC alone would be able to homogeneously nucleate, as their estimated vapor pressures (discussed below) are not low enough for that process. Therefore, we hypothesize that the ISOPOOH experiment led to SOA growth and the isoprene ones did not due to differences in the concentrations of pre-existing background nanoparticles between the experiments. Unfortunately, nanoparticle measurements were not performed due to space and flow constraints. Particles were detected and characterized after they grew to exceed the AMS size cutoff of \sim 50 nm diameter. It is also possible that some SOA was formed in the isoprene experiments, but that it was present in particle sizes below the AMS lower particle size transmission limit. Additionally, the upper limit concentration of 4,3-ISOPOOH consumed in experiments 2 and 21 can be estimated at $\frac{1}{3}$ and $\frac{1}{7}$ of the 42 ppb of 4,3-ISOPOOH that reacted away in this experiment. SOA formation, limited by a high loss rate of LVOC to the walls, will be dependent on the ISOPOOH oxidation rate (ppbv/min), which was much higher in the ISOPOOH experiment. The much smaller LVOC production combined with the strong sink to the walls may explain why the AMS did not detect aerosol mass above 50 nm in the other isoprene experiments.

SOA Composition. The AMS spectrum of the SOA is characterized by electron impact mass fragment ions with a high fraction of m/z 43, typical of fresh SOA (Figure S3) and m/z 29 (CHO⁺), typical of species with alcohol functional groups.³³ $C_2H_3O^+$ dominates m/z 43 and is thought to be associated with nonacid oxygenated functional groups.³⁸ The SOA measured by the AMS and the gas-phase condensing

species measured by the NO₃⁻-CIMS had consistent elemental composition: O:C of 0.90 \pm 0.2 (AMS) vs 1.1 \pm 0.1 (CIMS), and H:C of 1.75 \pm 0.25 (AMS) vs 2.1 \pm 0.1 (CIMS) (Figures 1c; eqns. and uncertainty in the Supporting Information). No detectable organic N was present in either the gas or the particle phase, supporting the lack of prevalence of high-NO pathways in these experiments.

Previous studies have shown that a key pathway for the formation of SOA in the low-NO isoprene system is the uptake of IEPOX followed by aerosol phase reactions. However, such uptake is thought to require particle liquid water and is accelerated by wet acidic sulfate particles, 14,39 which makes it unlikely to be active in our experiment. The lack of such uptake is also consistent with the fact that IEPOX concentrations in the chamber do not decrease when the photochemistry stops. The fraction of signal at m/z 82, $C_5H_6O^+$ $(f_{C_5H_6O})$ in the HR-AMS spectra is a good tracer of IEPOX-SOA⁴⁰ in wellcharacterized isoprene photochemical systems. $f_{\rm C,H_6O}$ observed for IEPOX-SOA (\sim 22 × 10⁻³) in laboratory and field studies is far higher than observed here. In this experiment, $f_{C_8H_8O}$ averages 0.9×10^{-3} (Figure 1d). This value is 25 times lower than expected for pure IEPOX-SOA, and below typical background values from locations not influenced by IEPOX-SOA (urban, biomass-burning plumes, nonbiogenic chamber SOA) and non-IEPOX forming isoprene studies (1.7–3.5 \times 10⁻³). Therefore, SOA formation from IEPOX uptake plays at most a minor role in this experiment.

LVOC Composition. A representative NO₃⁻-CIMS mass spectrum (averaged over 30 min of peak LVOC production) and a list of the identified ions are given in Figure 2 and Table S1. All of the LVOC are observed as clusters with the nitrate reagent ion ($[X\cdot NO_3]^-$). None of the LVOC was detected in appreciable quantity as deprotonated molecules, indicating that the cluster chemical ionization mechanism is efficient for these particular species. To our knowledge, this is the first published nitrate-ion spectrum of these isoprene/ISOPOOH oxidation products, although some of them have been identified in previous iodide-ion CIMS ambient data.⁴¹

Fourteen LVOC signals whose time series are indicative of condensation are highlighted in the mass spectrum and displayed in a pie chart (Figure 2b) representing the relative contributions of individual LVOC to the total amount of condensing LVOC. The total condensing gas-phase amount is dominated (\sim 75% by mixing ratio) by four ions, $C_5H_{10}O_5$

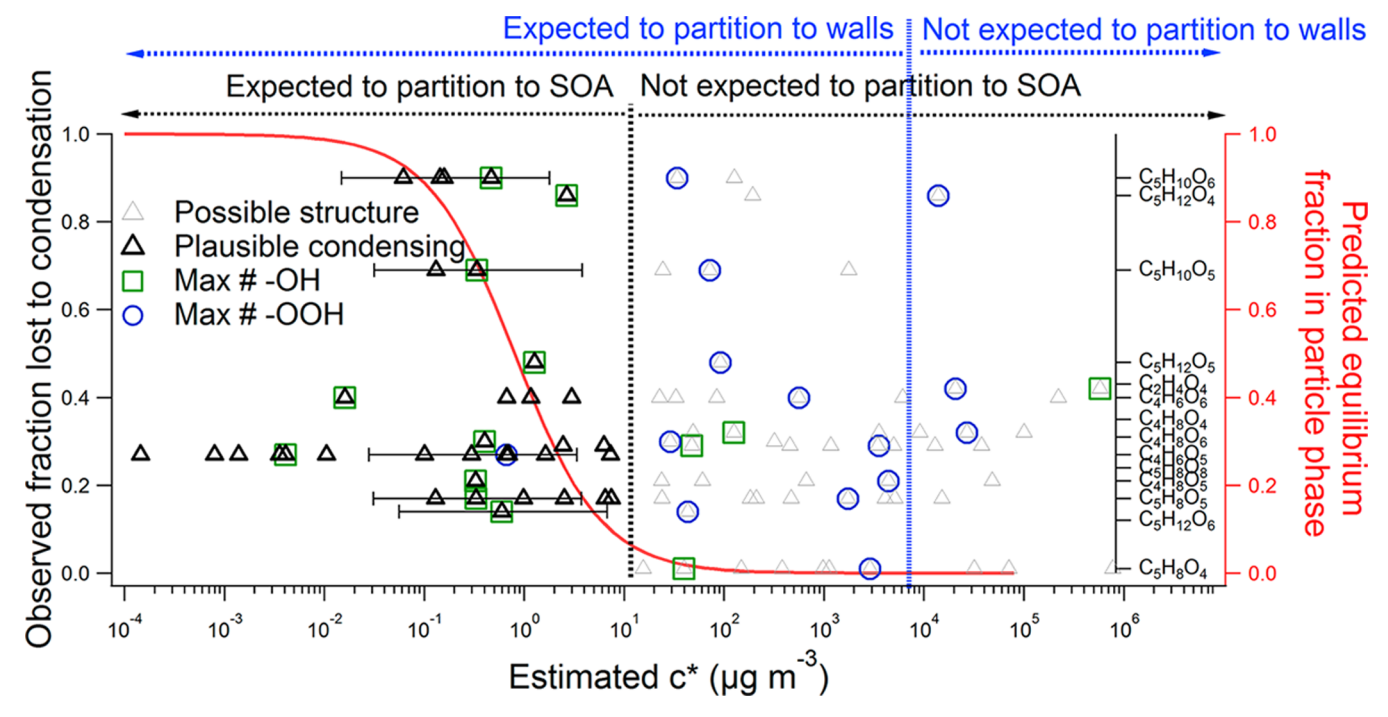


Figure 3. Left axis: fraction of gas-phase LVOC lost to aerosol uptake (estimated as described in main text) vs their estimated saturation concentrations (C*) from SIMPOL. Right axis: equilibrium particle-phase fraction for the peak aerosol concentration (0.85 µg m⁻³) vs C*. For each detected ion, a range of C^* was estimated for different possible functional group contents. Error bars are the estimated uncertainty (1σ) of SIMPOL.4

being the largest. All condensing LVOC are highly oxidized with O:C \geq 0.8 (0.8-1.2). Thirteen have a 4- or 5-carbon backbone, which is consistent for products arising from the oxidation of ISOPOOH and associated C5 compounds, ruling out gas-phase oligomerization reactions in their formation pathways. C₂H₄O₄ has a time series consistent with SOA formation, but its short carbon chain (and thus high vapor pressure) is consistent with condensation onto the aerosol via reactive uptake. The extent of condensation by reactive uptake of the C4 and C5 LVOC species is not known, however, we note that the observations can be explained from a simple condensation mechanism (i.e., no reactive uptake, see following section).

LVOC Functional Groups and Vapor Pressures. The fact that the LVOC are observed to condense onto the particle phase at SOA concentrations below 1 μ g m⁻³ indicates that their saturation concentrations (C^*) must be similar to or lower than the SOA concentration.²² Some information about the functional groups that are likely to be present on the LVOC can be obtained by estimating their C* based on their elemental composition and different functional group assumptions. A list of possible functional group combinations for each of the assigned elemental formulas is shown in Table S3. The SIMPOL.1 structure-activity relationship⁴² was used to estimate C^* .

The base vapor pressure for a 4- or 5-carbon structure (without oxygenated functional groups) is high (e.g., 0.72 atm. for isoprene), but decreases substantially with the addition of functional groups. Unlike, for example, terpene oxidation products, which have larger carbon numbers, isoprene oxidation products will only have low enough C* to condense if their oxygen is present in functional groups that efficiently reduce C*. We consider only O and H atoms because nitrogencontaining functional groups are not consistent with the

observed signals. Isoprene low-NO chemistry tends to produce neighboring hydroperoxyl and hydroxyl functional groups.⁴³ For example, C₅H₁₀O₅ has a double bond equivalency (DBE, the number of double bonds or rings) of one. It is unlikely that the C=C bond in ISOPOOH and associated OVOC survived oxidation, and thus we could assign one O to one epoxide, carboxyl, or carbonyl group. The four remaining O could be present as either two hydroperoxyl groups ($C^* = 1.8 \times 10^3 \,\mu g$ m⁻³), one hydroperoxyl and two hydroxyl groups ($C^* = 24 \mu g$ m^{-3}) or four hydroxyl groups ($C^* = 0.34 \mu g m^{-3}$). Thus, the presence of different functional groups can result in a difference of 4 orders-of-magnitude in C*. Although the addition of a hydroperoxyl group results in a larger decrease of C* than the addition of a hydroxyl group, the latter is more efficient at reducing C* per O atom. The most likely identity of the condensing C5H10O5 species is thus a C5 epoxyl- or carbonyltetrol, although a C₅ epoxyl- (or carbonyl-) hydroperoxydiol, and C5 carboxyl triol are also plausible given the fact that C* estimation methods have uncertainties of about 1 order of magnitude.⁴⁴ On the other hand, a carbonyl dihydroperoxide is not expected to partition through simple condensation based on vapor pressure, although it could still contribute to the particle phase via heterogeneous reactive uptake reactions. The large number of possible structures and variability of associated C* values demonstrate the difficulty of parametrizing these species' wall and aerosol loss rates based on bulk properties such as the number of oxygen and carbon atoms. 45

Figure 3 illustrates the results of this method for all condensing LVOC. Structures containing the maximum number of -OOH groups consistent with the measured composition tend to be too volatile to result in the observed condensing behavior. On the other hand, structures containing the maximum number of -OH groups are consistent with condensation at SOA $\sim 1 \ \mu g \ m^{-3}$ in most cases. As for the case

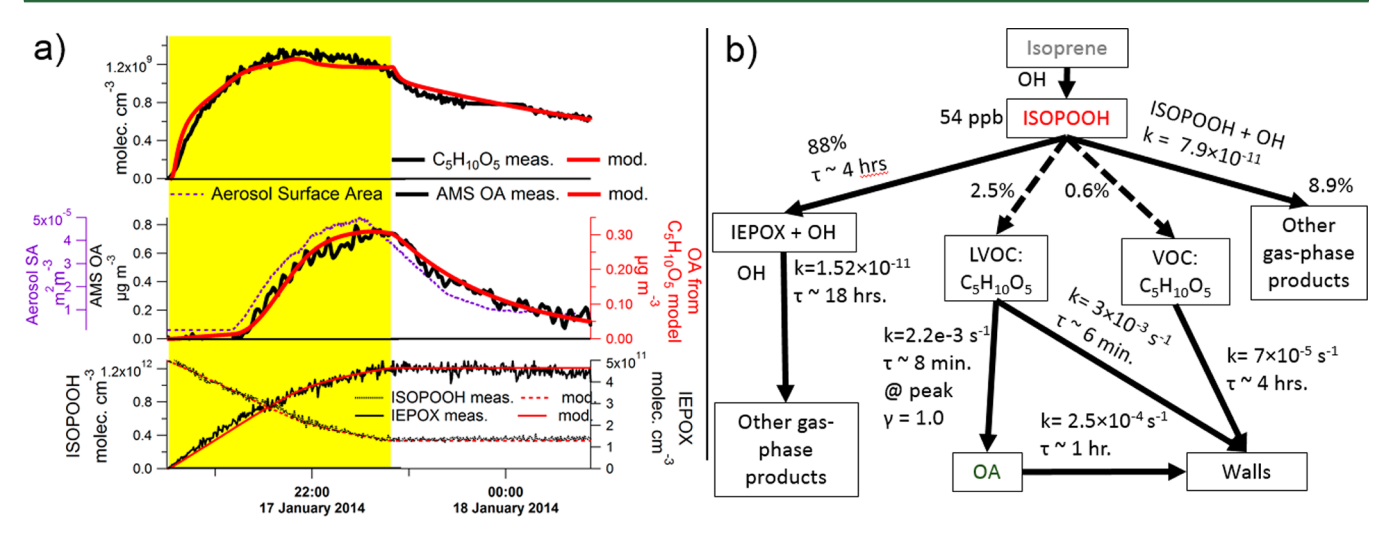


Figure 4. (a) Time series of modeled (red) and measured (black) gas and aerosol concentrations for the largest LVOC by contribution to SOA mass, C₅H₁₀O₅. The model SOA (middle, right axis) gives the fractional contribution of C₅H₁₀O₅ to the aerosol and the surface area has been binomially smoothed across 10 points. The LVOC was fit with two modeled isomers: one with $\gamma_{SOA} = 1.0$, $k_{wall} = 3.0 \times 10^{-3} \text{ s}^{-1}$ and a branching ratio of 2.5%; and another with $\gamma_{SOA} = 0$, $k_{wall} = 7.0 \times 10^{-5}$, and a branching ratio of 0.6%. (b) Schematic of the kinetic box model used to simulate the production of LVOC C₅H₁₀O₅ and its losses to organic aerosol (OA) and chamber walls. The dashed lined represents the proposed LVOC formation pathways. Isoprene is shown for reference, but was not present in the main experiment discussed in this work. Rate coefficients are in units of molec. cm⁻³ s⁻¹ unless otherwise specified.

of C₅H₁₀O₅, some structures containing a mixture of -OH and -OOH may also condense under the conditions of our experiment. Thus, we do not need to invoke oligomerization reactions to explain the observed SOA growth. Note that two or more isomers of differing volatility may comprise some of the detected signals. Unfortunately, a more precise determination of the molecular structures of the condensing LVOC is not possible with the available data.

Model Results. To better understand the observed LVOC temporal behavior, we implemented a kinetic box model. Model results for C₅H₁₀O₅ are compared to experimental data in Figure 4a and its structure and key parameters are shown in Figure 4b and Table S2. The model was constrained to match all observed variables, while keeping its structure as simple as possible and the number of fitted parameters as low as possible. It was possible to reproduce the behavior of the largestconcentration and SOA-condensing LVOC assuming that LVOC were formed from ISOPOOH + OH and were lost to the chamber walls and to the aerosol.

The initial rise of the LVOC concentrations allows constraining the extent to which these species are predominantly formed from ISOPOOH + OH, or from the oxidation of IEPOX (or other first generation products) by OH. Figure S4a,b show the relative rise in concentration from the LVOC and IEPOX before the appearance of SOA, as well as the expected time dependences for first, second, and later generation products of ISOPOOH. The rate coefficient used for OH oxidation of IEPOX and subsequent IEPOX products is $1.52 \times 10^{-11} \text{ cm}^3 \text{ molec.}^{-1} \text{ s}^{-1}$, as recently reported for cis- β IEPOX (the isomer with the largest rate coefficient, providing an upper bound for the reaction rate). 12 The time when LVOC and IEPOX rise represents a period when only one source and one sink (chamber walls; shown in Figure S5) are dominant. When LVOC are modeled as first generation products of ISOPOOH + OH, the model curve lies in the middle of the measured traces and follows almost the same path as the IEPOX measurement (as expected since IEPOX is a first generation product of ISOPOOH+OH). The later generation

product assumptions produce traces that are significantly delayed, then exhibit a sharper relative increase later in this period. Thus, we conclude that most LVOC are formed as minor products of the ISOPOOH+OH reaction. Two LVOC lie in between the first and second generation curves in Figure S4b. This may just be due to experimental variability and instrument noise, as several LVOC lay just as far to the other side of the first generation curve. Potentially a few LVOC may have a contribution of later generation reactions.

Next, we turn our attention to constraining the uptake coefficient for LVOC uptake to SOA (γ_{SOA}) and the wall loss rate (k_{wall}) (Figure S4d). The time evolution of this experiment contains information to potentially constrain these values separately due to drastic changes in their relative importance within different time periods. First, there is an initial period (20:30-21:10 UTC) before SOA appears when wall loss dominates as a sink, then a second period (21:30-end) when SOA is present in variable concentrations.

An aerosol uptake coefficient $\gamma_{SOA} = 1.0 \pm 0.1$, a wall loss rate of $k_{wall} = 3.0 \times 10^{-3} \text{ s}^{-1} \pm 7.5 \times 10^{-4} \text{ s}^{-1}$, and an ISOPOOH + OH branching ratio for $C_5H_{10}O_5$ of 2.5% \pm 0.6% best reproduces the observed time series for the SOA-condensing C₅H₁₀O₅ isomer. These values correspond to a first-order uptake rate (lifetime) of $k_{SOA} \sim 2.2 \times 10^{-3} \text{ s}^{-1} (\sim 8 \text{ min})$ at the peak of OA surface area and a wall-loss time scale of ~6 min. A detailed explanation of the parameter estimation method and related uncertainty is given in the SI.

The time-dependent LVOC behavior after the lights are turned off shows substantial variations in the LVOC relative loss rates to wall plus aerosol (Figure S4c and d, respectively). The measured LVOC traces are compared with the results of several model runs for multiple values of $\gamma_{\rm SOA}$ and $k_{\rm wall}$ (Figure S4d). The majority of traces lie within a relatively narrow range of uptake coefficients ($k_{\text{wall}} = 1.0 \times 10^{-4} \text{ to } \sim 5.0 \times 10^{-3} \text{ and}$ $\gamma_{SOA} \sim 0.5-1$).

We note that most detected LVOC reach a plateau ~2 h after the lights are turned off. This could be due to two different reasons: (a) equilibrium is being reached and a substantial gas-

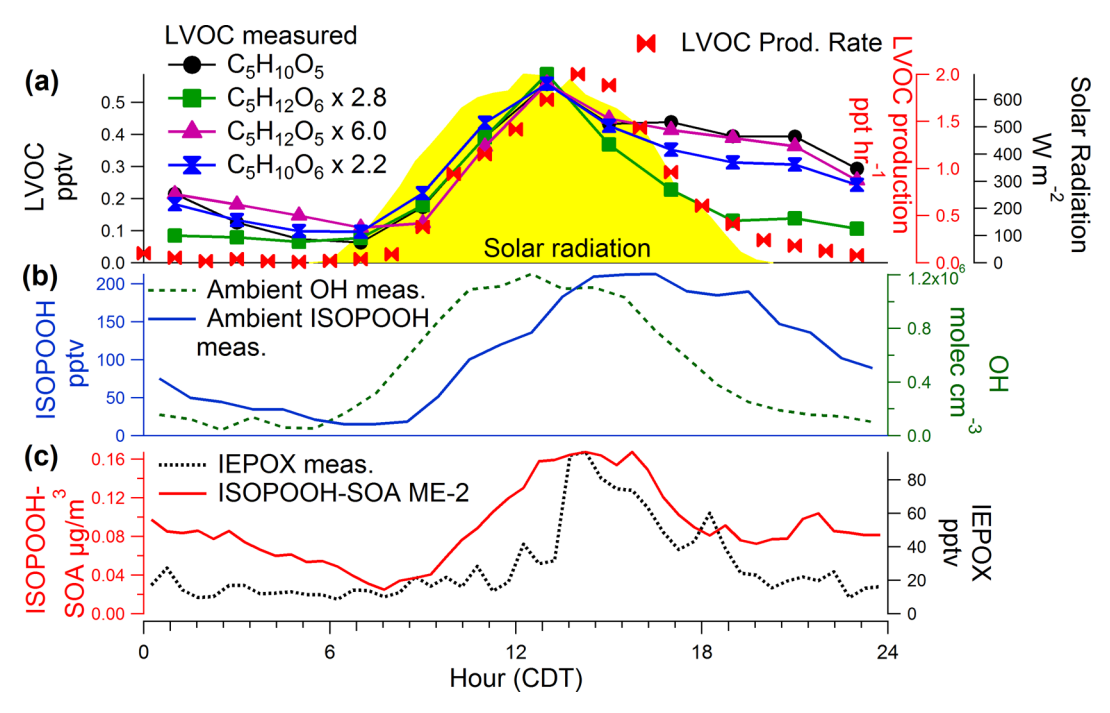


Figure 5. Diurnal cycles of ambient measurements during the SOAS field study from a 10-day period beginning 22 June 2013: (a) key LVOC identified in the laboratory; and (b) OH and ISOPOOH. Also shown in panel (a) is the LVOC production rate (k[ISOPOOH][OH]) multiplied by a yield of ~1%. All of the diurnal cycles peak around 13:00 CDT when solar radiation and OH are at peak levels. (c) ISOPOOH SOA estimated with factor analysis of ambient AMS data and ambient IEPOX. ISOPOOH and OH were binomially smoothed over five or two data points, respectively, before diurnal averaging. The time scale of aerosol uptake is estimated at ~4 min.

phase fraction remains for all LVOC; or (b) the presence of (at least) one condensing and one noncondensing isomer for each compound detected. Gas-wall partitioning for oxidized species can be approximately modeled with an equivalent OA mass of \sim 5 mg m^{-3.46,47} Since these LVOC are observed to condense on OA concentrations 10^4 times lower, their C^* must be of the order of 1 μ g m⁻³, and a substantial gas-phase fraction cannot remain in equilibrium with the high equivalent wall concentrations. Thus, we conclude that the presence of at least one noncondensing isomer is the most likely explanation, which is consistent with the range of possible C* shown in Figure 3. For example, the observed time series of C₅H₁₀O₅ (Figure 4b) could only be matched by simulating the formation of two isomers, one of which is lost to the aerosol and one of which was not (Figure S6). The noncondensing isomer was fit with a $k_{\text{wall}} = 7.0 \times 10^{-5} \ (\tau_{\text{wall}} \sim 4 \ \text{h})$. Branching ratios of 2.5% and 0.6% (Table S2) for the condensing and noncondensing isomers, respectively, provided a quantitative match with the observations.

The second and third highest aerosol-contributing LVOC, C₅H₁₂O₅ and C₅H₁₂O₆ were also modeled and are shown in Figures S7 and S8 along with their uptake coefficients. These wall loss rates are consistent and are in the expected range for low volatility species based on previous modeling studies of experiments in the Caltech chamber and other facilities (Figure S9).45 C5H12O6 is the largest observed signal in the gas-phase spectrum, contributing the third-largest amount of mass to SOA. Previous works 10,18,48 have proposed that this species could possibly form from the gas-phase oxidation of ISOPOOH by OH with a subsequent reaction with O2 and HO2, resulting in a C₅ dihydroxy dihydroperoxide (Figure S10), although this species was not observed in that study. However, the time dependence of the C₅H₁₂O₆ increase (Figure S8) appears

intermediate between a first-generation and second-generation mechanism, suggesting multiple potential formation pathways.

Ambient Observations. The 14 condensing species detected during the ISOPOOH chamber experiment were also observed in the ambient environment by the same NO₃⁻-CIMS (with a shorter (0.7 m) inlet) at the Centreville, AL supersite during the SOAS campaign in summer 2013. The site was a rural, mixed-forest site where a substantial fraction of isoprene oxidation proceeds through the low-NO isoprene pathway. The diurnal cycles for the four most abundant LVOC are shown in Figure 5a. ISOPOOH concentrations show a broad maximum, peaking at 16:00 (CDT) as shown in Figure 5b. These LVOC show temporal behavior consistent with isoprene + OH oxidation products, and not of other biogenic hydrocarbons, such as monoterpenes, or of NO₃ chemistry products, which peaked at night. The diurnal cycle of modeled LVOC production rates is also presented in Figure 5a. The production is estimated as

$$P[LVOC] = Y_{LVOC}k_{ISOPOOH-OH}[ISOPOOH][OH]$$
 (1)

where Y_{LVOC} is the total LVOC yield determined from the chamber experiments, and the [ISOPOOH] and [OH] concentrations are from the actual SOAS measurements (Figure 5b). The estimated production rate is consistent with the LVOC diurnal profiles observed in the atmosphere. The main loss of the LVOC is expected to be condensation onto the aerosol. Scaling the time scales observed in the chamber by the ratio of the surface areas provides a time constant for this process of the order of 30 min, which is consistent with the rapid decrease in LVOC concentrations in the afternoon.

We also performed a Positive Matrix Factorization analysis of the ambient AMS SOAS data in which we constrained the spectrum from FIXCIT ISOPOOH-SOA. The details and results of this analysis are given in the SI and Figure 5c,

respectively. We obtained an average ISOPOOH-SOA SOAS ambient concentration of \sim 95 ng m⁻³, which accounts for \sim 2% of the observed ambient OA. This is consistent with our estimated peak concentration of 85 ng m⁻³ by integrating the area under the production rate curve in Figure 5a and assuming a comparatively slow loss (\sim 12 h) via dry deposition.⁴⁹

A full model for the observed ambient traces would also need to consider surface deposition as well as growth of the boundary layer and entrainment at its top, ⁵⁰ which is beyond the scope of this work. The fact that some LVOC signals persist into the night when production should be much slower suggests that some fraction of the signal is composed of more volatile noncondensing isomers.

Atmospheric Implications. Assuming that all of the maximum chamber SOA peak concentration of 0.85 μ g m⁻³ was due to LVOC condensation from oxidation of 42 ppbv of ISOPOOH, we obtain a wall-loss corrected SOA mass yield of 4.2% from 4,3-ISOPOOH. The relatively large gas-phase loss to the walls (Figure S11) results from the large ratio of wall surface area to aerosol surface area. At the peak of the aerosol surface area, this ratio is $1:2 \times 10^{-5}$. The total estimated uncertainty of the SOA yield has contributions from the instruments, aerosol surface area, standard impurities, and wall loss correction uncertainties. We estimate the overall uncertainty on the SOA yield from 4,3-ISOPOOH via the LVOC pathway as a factor of 2.5. Compared to values in a previous study of the effect of seed-to-chamber surface area ratio on aerosol mass yields (Table 1 in ref⁴⁵), the surface area ratio in this study is in a range in which vapor wall deposition has been shown to reduce SOA yields. These small SOA concentrations (<1 μ g m⁻³) are unusual for most SOA-focused experiments at Caltech or other chambers. Our results suggest that SOA yields determined at low "atmospherically relevant" SOA loadings may have significant low biases if vapor losses to walls are not accounted for (Figure S12).^{51,52}

Under the assumption that all SOA in the chamber experiment was formed from the oxidation of 4,3-ISOPOOH (see above and SI text for possible role of other OVOC present in chamber), we estimate the implied global SOA production rates via this mechanism. First, we estimate the 4,3-ISOPOOH yield from isoprene. The total ISOPOOH yield from isoprene + OH + O_2 + H O_2 reactions is estimated to be >75% (molar) yield. Here, we assume the 4,3-ISOPOOH isomer to compose ~40% (±10%) of ambient ISOPOOH production. 11,53 We do not know the LVOC yield from 1,2-ISOPOOH. Thus, the non-IEPOX SOA yield from isoprene via 4,3-ISOPOOH is estimated at 2.3%. If 1,2-ISOPOOH has the same yield of condensing SOA as observed in this experiment, the calculated non-IEPOX SOA yield from isoprene would be 5.8%. To estimate the global SOA production we use the estimated fraction of isoprene peroxy radicals reacting with HO₂ (43%),⁵⁴ giving a final global production of 5 Tg yr⁻¹ (via 4,3-ISOPOOH only) of SOA, or \sim 3.3% of the estimated annual SOA production from all sources of \sim 150 Tg yr⁻¹. This non-IEPOX SOA source is comparable in magnitude to the maximum potential SOA formation of the ELVOC pathway (6.5 Tg yr⁻¹)²³ though not in nucleation potential, meaning the new SOA formation pathway is likely to be atmospherically significant. Furthermore, because this SOA was observed to grow nanoparticles and to condense on OA below 1 μ g m⁻³ at room temperature, this pathway would be operative in clean ambient environments

with low OA concentrations and especially contribute to the growth of nanoparticles, which traditional SVOCs cannot do. ⁵⁵

Although IEPOX forms from isoprene at high yields, its uptake into atmospheric aerosol is often at a slow rate, ³⁹ leading to large losses to dry deposition and OH reaction. ⁴⁹ The non-IEPOX SOA source proposed in this work forms from small amounts of gas-phase LVOC with high yields, as the LVOCs rapidly condense onto existing particulate matter. It has recently been proposed ¹⁵ that IEPOX uptake may only explain half of aerosol formed from low-NO isoprene oxidation; the SOA pathway in this work may account for a fraction of that missing SOA source.

Future laboratory studies should investigate the molecular identities and formation mechanisms of these LVOC, the effect of conditions such as temperature and aerosol water, and the potential formation of LVOC from other isoprene reaction pathways. Of special interest is the yield of LVOC and SOA from 1,2-ISOPOOH. In addition, the lifetime of the SOA produced via this chemistry should be investigated. ^{56,57}

ASSOCIATED CONTENT

Supporting Information

The Supporting Information is available free of charge on the ACS Publications website at DOI: 10.1021/acs.est.5b02031.

Detailed information on vapor pressure calculations, details of the kinetic box model, AMS organic aerosol spectra, detailed model results for additional LVOC species, and detailed information on wall losses (PDF)

AUTHOR INFORMATION

Corresponding Authors

*(J.L.J.) Phone: 303-492-3557; fax: 303-492-1149; e-mail: jose. jimenez@colorado.edu.

*(M.R.C.) Phone: (978) 663-9500; e-mail: mrcana@aerodyne.

Present Addresses

[%]Harvard John A. Paulson School of Engineering and Applied Sciences, Department of Chemistry and Chemical Biology, Harvard University, Cambridge, Massachusetts, United States ^fAtmospheric Chemistry and Dynamics Laboratory, NASA Goddard Space Flight Center, Greenbelt, Maryland, United States and Joint Center for Earth Systems Technology, University of Maryland Baltimore County, Baltimore, Maryland, United States

Notes

The authors declare no competing financial interest

ACKNOWLEDGMENTS

This work was supported by grants NSF AGS-1243354, 1243356, 1247421, and 1246918, NOAA NA13OAR4310063, and DOE (BER/ASR) DE-SC0011105. J.K. is grateful for fellowships from CIRES, CU Graduate School, and EPA STAR (FP-91770901-0). We are grateful to the many contributions to the FIXCIT study made by the staff and students of the Wennberg and Seinfeld groups, and fellow participants. We also thank Profs. P. Ziemann and B. Aumount for useful discussions.

REFERENCES

(1) Pope, C. A., III; Dockery, D. W. Health Effects of Fine Particulate Air Pollution: Lines that Connect. *J. Air Waste Manage. Assoc.* **2006**, 56, 709–742.

- (2) Myhre, G.; Shindell, D.; Bréon, F.-M.; Collins, W.; Fuglestvedt, J.; Huang, J.; Koch, D.; Lamarque, J.-F.; Lee, D.; Mendoza, B.; et al. Anthropogenic and Natural Radiative Forcing. In Climate Change 2013: The Physical Science Basis. Contribution of Working Group I to the Fifth Assessment Report of the Intergovernmental Panel on Climate Change; Stocker, T. F., Ed.; Cambridge University Press: Cambridge, 2013.
- (3) Jimenez, J. L.; Canagaratna, M. R.; Donahue, N. M.; Prevot, A. S. H.; Zhang, Q.; Kroll, J. H.; DeCarlo, P. F.; Allan, J. D.; Coe, H.; Ng, N. L.; et al. Evolution of organic aerosols in the atmosphere. *Science* **2009**, 326, 1525–1529.
- (4) Hallquist, M.; Wenger, J.; Baltensperger, U.; Rudich, Y.; Simpson, D.; Claeys, M.; Dommen, J.; Donahue, N.; George, C.; Goldstein, A.; et al. The formation, properties and impact of secondary organic aerosol: current and emerging issues. *Atmos. Chem. Phys.* **2009**, *9*, 5155–5236.
- (5) Heald, C. L.; Coe, H.; Jimenez, J. L.; Weber, R. J.; Bahreini, R.; Middlebrook, a. M.; Russell, L. M.; Jolleys, M.; Fu, T.-M.; Allan, J. D.; et al. Exploring the vertical profile of atmospheric organic aerosol: comparing 17 aircraft field campaigns with a global model. *Atmos. Chem. Phys.* **2011**, *11*, 12673–12696.
- (6) Tsigaridis, K.; Daskalakis, N.; Kanakidou, M.; Adams, P. J.; Artaxo, P.; Bahadur, R.; Balkanski, Y.; Bauer, S. E.; Bellouin, N.; Benedetti, A.; et al. The AeroCom evaluation and intercomparison of organic aerosol in global models. *Atmos. Chem. Phys.* **2014**, *14*, 10845—10895.
- (7) Guenther, A. B.; Jiang, X.; Heald, C. L.; Sakulyanontvittaya, T.; Duhl, T.; Emmons, L. K.; Wang, X. The Model of Emissions of Gases and Aerosols from Nature version 2.1 (MEGAN2.1): an extended and updated framework for modeling biogenic emissions. *Geosci. Model Dev.* 2012, 5, 1471–1492.
- (8) Guenther, A.; Nicholas, C.; Erickson, D.; Fall, R.; Geron, C.; Gradel, T.; Harley, P.; Klinger, L.; Lerdau, M.; Mckay, W. A.; et al. A global model of natural volatile organic compound emissions. *J. Geophys. Res.* **1995**, *100*, 8873–8892.
- (9) Crutzen, P. J.; Williams, J.; Po, U.; Hoor, P.; Fischer, H.; Warneke, C.; Holzinger, R.; Hansel, A.; Lindinger, W.; Scheeren, B.; et al. High spatial and temporal resolution measurements of primary organics and their oxidation products over the tropical forests of Surinam. *Atmos. Environ.* **2000**, *34*, 1161–1165.
- (10) Paulot, F.; Crounse, J. D.; Kjaergaard, H. G.; Kürten, A.; St Clair, J. M.; Seinfeld, J. H.; Wennberg, P. O. Unexpected epoxide formation in the gas-phase photooxidation of isoprene. *Science* **2009**, 325, 730–733.
- (11) Rivera-Rios, J. C.; Nguyen, T. B.; Crounse, J. D.; Jud, W.; St. Clair, J. M.; Mikoviny, T.; Gilman, J. B.; Lerner, B. M.; Kaiser, J. B.; de Gouw, J.; et al. Conversion of hydroperoxides to carbonyls in field and laboratory instrumentation: Observational bias in diagnosing pristine versus anthropogenically controlled atmospheric chemistry. *Geophys. Res. Lett.* **2014**, *41*, 8645–8651.
- (12) Bates, K. H.; Crounse, J. D.; St Clair, J. M.; Bennett, N. B.; Nguyen, T. B.; Seinfeld, J. H.; Stoltz, B. M.; Wennberg, P. O. Gas phase production and loss of isoprene epoxydiols. *J. Phys. Chem. A* **2014**, *118*, 1237–1246.
- (13) Xu, L.; Guo, H.; Boyd, C. M.; Klein, M.; Bougiatioti, A.; Cerully, K. M.; Hite, J. R.; Isaacman-VanWertz, G.; Kreisberg, N. M.; Knote, C.; et al. Effects of anthropogenic emissions on aerosol formation from isoprene and monoterpenes in the southeastern United States. *Proc. Natl. Acad. Sci. U. S. A.* 2015, 112, 37–42.
- (14) Nguyen, T. B.; Coggon, M. M.; Bates, K. H.; Zhang, X.; Schwantes, R. H.; Schilling, K. A.; Loza, C. L.; Flagan, R. C.; Wennberg, P. O.; Seinfeld, J. H. Organic aerosol formation from the reactive uptake of isoprene epoxydiols (IEPOX) onto non-acidified inorganic seeds. *Atmos. Chem. Phys.* **2014**, *14*, 3497–3510.
- (15) Liu, Y.; Kuwata, M.; Strick, B. F.; Geiger, F. M.; Thomson, R. J.; McKinney, K. A.; Martin, S. T.; Geiger, F. M.; McKinney, K. A.; Martin, S. T. Uptake of Epoxydiol Isomers Accounts for Half of the Particle-Phase Material Produced from Isoprene Photooxidation via the HO2 Pathway. *Environ. Sci. Technol.* **2015**, *49*, 250–258.

- (16) Kjaergaard, H. G.; Knap, H. C.; Ørnsø, K. B.; Jørgensen, S.; Crounse, J. D.; Paulot, F.; Wennberg, P. O. Atmospheric fate of methacrolein. 2. Formation of lactone and implications for organic aerosol production. *J. Phys. Chem. A* **2012**, *116*, 5763–5768.
- (17) Lin, Y.-H.; Zhang, H.; Pye, H. O. T.; Zhang, Z.; Marth, W. J.; Park, S.; Arashiro, M.; Cui, T.; Budisulistiorini, S. H.; Sexton, K. G.; et al. Epoxide as a precursor to secondary organic aerosol formation from isoprene photooxidation in the presence of nitrogen oxides. *Proc. Natl. Acad. Sci. U. S. A.* **2013**, *110*, *6718–6723*.
- (18) Kroll, J. H.; Ng, N. L.; Murphy, S. M.; Flagan, R. C.; Seinfeld, J. H. Secondary Organic Aerosol Formation from Isoprene Photooxidation. *Environ. Sci. Technol.* **2006**, *40*, 1869–1877.
- (19) Chan, A. W. H.; Chan, M. N.; Surratt, J. D.; Chhabra, P. S.; Loza, C. L.; Crounse, J. D.; Yee, L. D.; Flagan, R. C.; Wennberg, P. O.; Seinfeld, J. H. Role of aldehyde chemistry and NOx concentrations in secondary organic aerosol formation. *Atmos. Chem. Phys.* **2010**, *10*, 7169—7188
- (20) Spracklen, D. V.; Jimenez, J. L.; Carslaw, K.; Worsnop, D. R.; Evans, M. J.; Mann, G. W.; Zhang, Q.; Canagaratna, M. R.; Allan, J.; Coe, H.; et al. Aerosol mass spectrometer constraint on the global secondary organic aerosol budget. *Atmos. Chem. Phys.* **2011**, *11*, 12109–12136.
- (21) Pankow, J. F. An absorption model of gas/particle partitioning of organic compounds in the atmosphere. *Atmos. Environ.* **1994**, 28, 185–188.
- (22) Donahue, N. M.; Robinson, A. L.; Stanier, C. O.; Pandis, S. N. Coupled partitioning, dilution, and chemical aging of semivolatile organics. *Environ. Sci. Technol.* **2006**, *40*, 2635–2643.
- (23) Ehn, M.; Thornton, J. A.; Kleist, E.; Sipilä, M.; Junninen, H.; Pullinen, I.; Springer, M.; Rubach, F.; Tillmann, R.; Lee, B.; et al. A large source of low-volatility secondary organic aerosol. *Nature* **2014**, 506, 476–479.
- (24) Jokinen, T.; Sipilä, M.; Richters, S.; Kerminen, V.-M.; Paasonen, P.; Stratmann, F.; Worsnop, D.; Kulmala, M.; Ehn, M.; Herrmann, H.; et al. Rapid Autoxidation Forms Highly Oxidized RO2 Radicals in the Atmosphere. *Angew. Chem., Int. Ed.* **2014**, *53*, 14596–14600.
- (25) Crounse, J. D.; Nielsen, L. B.; Jørgensen, S.; Kjaergaard, H. G.; Wennberg, P. O. Autoxidation of Organic Compounds in the Atmosphere. J. Phys. Chem. Lett. 2013, 4, 3513–3520.
- (26) Nguyen, T. B.; Crounse, J. D.; Schwantes, R. H.; Teng, A. P.; Bates, K. H.; Zhang, X.; St. Clair, J. M.; Brune, W. H.; Tyndall, G. S.; Keutsch, F. N.; et al. Overview of the Focused Isoprene eXperiment at the California Institute of Technology (FIXCIT): mechanistic chamber studies on the oxidation of biogenic compounds. *Atmos. Chem. Phys.* **2014**, *14*, 13531–13549.
- (27) Yatavelli, R. L. N.; Lopez-Hilfiker, F.; Wargo, J. D.; Kimmel, J. R.; Cubison, M. J.; Bertram, T. H.; Jimenez, J. L.; Gonin, M.; Worsnop, D. R.; Thornton, J. A. A Chemical Ionization High-Resolution Time-of-Flight Mass Spectrometer Coupled to a Micro Orifice Volatilization Impactor (MOVI-HRToF-CIMS) for Analysis of Gas and Particle-Phase Organic Species. *Aerosol Sci. Technol.* **2012**, *46*, 1313–1327.
- (28) Junninen, H.; Ehn, M.; Petäjä, T.; Luosujärvi, L.; Kotiaho, T.; Kostiainen, R.; Rohner, U.; Gonin, M.; Fuhrer, K.; Kulmala, M.; et al. A high-resolution mass spectrometer to measure atmospheric ion composition. *Atmos. Meas. Tech.* **2010**, *3*, 1039–1053.
- (29) Eisele, F.; Tanner, D. Measurement of the gas phase concentration of H2SO4 and methane sulfonic acid and estimates of H2SO4 production and loss in the atmosphere. *J. Geophys. Res.* **1993**, *98*, 9001–9010.
- (30) Ehn, M.; Junninen, H.; Petäjä, T.; Kurtén, T.; Kerminen, V.-M.; Schobesberger, S.; Manninen, H. E.; Ortega, I. K.; Vehkamäki, H.; Kulmala, M.; et al. Composition and temporal behavior of ambient ions in the boreal forest. *Atmos. Chem. Phys.* **2010**, *10*, 8513–8530.
- (31) Ehn, M.; Kleist, E.; Junninen, H.; Petäjä, T.; Lönn, G.; Schobesberger, S.; Dal Maso, M.; Trimborn, a.; Kulmala, M.; Worsnop, D. R.; et al. Gas phase formation of extremely oxidized pinene reaction products in chamber and ambient air. *Atmos. Chem. Phys.* **2012**, *12*, 5113–5127.

- (32) Decarlo, P. F.; Kimmel, J. R.; Trimborn, A.; Northway, M. J.; Jayne, J. T.; Aiken, A. C.; Gonin, M.; Fuhrer, K.; Horvath, T.; Docherty, K. S.; et al. Field-Deployable, High-Resolution, Time-of-Flight Aerosol Mass Spectrometer. *Anal. Chem.* **2006**, *78*, 8281–8289.
- (33) Canagaratna, M. R.; Jimenez, J. L.; Kroll, J. H.; Chen, Q.; Kessler, S. H.; Massoli, P.; Hildebrandt Ruiz, L.; Fortner, E.; Williams, L. R.; Wilson, K. R.; et al. Elemental ratio measurements of organic compounds using aerosol mass spectrometry: characterization, improved calibration, and implications. *Atmos. Chem. Phys.* **2015**, *15*, 253–272.
- (34) Crounse, J.; McKinney, K.; Kwan, A. J.; Wennberg, P. O. Measurement of gas-phase hydroperoxides by chemical ionization mass spectrometry. *Anal. Chem.* **2006**, *78*, 6726–6732.
- (35) St Clair, J. M.; McCabe, D. C.; Crounse, J. D.; Steiner, U.; Wennberg, P. O. Chemical ionization tandem mass spectrometer for the in situ measurement of methyl hydrogen peroxide. *Rev. Sci. Instrum.* **2010**, *81*, 094102–094106.
- (36) Middlebrook, A. M.; Bahreini, R.; Jimenez, J. L.; Canagaratna, M. R. Evaluation of Composition-Dependent Collection Efficiencies for the Aerodyne Aerosol Mass Spectrometer using Field Data. *Aerosol Sci. Technol.* **2012**, *46*, 258–271.
- (37) Bahreini, R.; Ervens, B.; Middlebrook, A. M.; Warneke, C.; de Gouw, J. A.; DeCarlo, P. F.; Jimenez, J. L.; Brock, C. a.; Neuman, J. A.; Ryerson, T. B.; et al. Organic aerosol formation in urban and industrial plumes near Houston and Dallas, Texas. *J. Geophys. Res.* **2009**, *114*, D00E16
- (38) Ng, N. L.; Canagaratna, M. R.; Jimenez, J. L.; Chhabra, P. S.; Seinfeld, J. H.; Worsnop, D. R. Changes in organic aerosol composition with aging inferred from aerosol mass spectra. *Atmos. Chem. Phys.* **2011**, *11*, 6465–6474.
- (39) Gaston, C. J.; Riedel, T. P.; Zhang, Z.; Gold, A.; Surratt, J. D.; Thornton, J. A. Reactive uptake of an isoprene-derived epoxydiol to submicron aerosol particles. *Environ. Sci. Technol.* **2014**, *48*, 11178–11186
- (40) Hu, W. W.; Campuzano-Jost, P.; Palm, B. B.; Day, D. A.; Ortega, A. M.; Hayes, P. L.; Krechmer, J. E.; Chen, Q.; Kuwata, M.; Liu, Y. J.; et al. Characterization of a real-time tracer for Isoprene Epoxydiols-derived Secondary Organic Aerosol (IEPOX-SOA) from aerosol mass spectrometer measurements. *Atmos. Chem. Phys. Discuss.* **2015**, *15*, 11223–11276.
- (41) Lee, B. H.; Lopez-Hilfiker, F. D.; Mohr, C.; Kurtén, T.; Worsnop, D. R.; Thornton, J. A. An iodide-adduct high-resolution time-of-flight chemical-ionization mass spectrometer: application to atmospheric inorganic and organic compounds. *Environ. Sci. Technol.* **2014**, *48*, 6309–6317.
- (42) Pankow, J. F.; Asher, W. E. SIMPOL.1: a simple group contribution method for predicting vapor pressures and enthalpies of vaporization of multifunctional organic compounds. *Atmos. Chem. Phys.* **2008**, *8*, 2773–2796.
- (43) Atkinson, R. Gas-Phase Tropospheric Chemistry of Volatile Organic Compounds: 1. Alkanes and Alkenes. *J. Phys. Chem. Ref. Data* 1997, 26, 215–290.
- (44) Barley, M. H.; McFiggans, G. The critical assessment of vapour pressure estimation methods for use in modelling the formation of atmospheric organic aerosol. *Atmos. Chem. Phys.* **2010**, *10*, 749–767.
- (45) Zhang, X.; Cappa, C. D.; Jathar, S. H.; McVay, R. C.; Ensberg, J. J.; Kleeman, M. J.; Seinfeld, J. H. Influence of vapor wall loss in laboratory chambers on yields of secondary organic aerosol. *Proc. Natl. Acad. Sci. U. S. A.* **2014**, *111*, 5802–5807.
- (46) Matsunaga, A.; Ziemann, P. J. Gas-Wall Partitioning of Organic Compounds in a Teflon Film Chamber and Potential Effects on Reaction Product and Aerosol Yield Measurements. *Aerosol Sci. Technol.* **2010**, *44*, 881–892.
- (47) Yeh, G. K.; Ziemann, P. J. Identification and yields of 1,4-hydroxynitrates formed from the reactions of C8-C16 n-alkanes with OH radicals in the presence of NO(x). *J. Phys. Chem. A* **2014**, *118*, 8797–8806.
- (48) Surratt, J. D.; Murphy, S. M.; Kroll, J. H.; Ng, N. L.; Hildebrandt, L.; Sorooshian, A.; Szmigielski, R.; Vermeylen, R.;

- Maenhaut, W.; Claeys, M.; et al. Chemical composition of secondary organic aerosol formed from the photooxidation of isoprene. *J. Phys. Chem. A* **2006**, *110*, 9665–9690.
- (49) Nguyen, T. B.; Crounse, J. D.; Teng, A. P.; St. Clair, J. M.; Paulot, F.; Wolfe, G. M.; Wennberg, P. O. Rapid deposition of oxidized biogenic compounds to a temperate forest. *Proc. Natl. Acad. Sci. U. S. A.* **2015**, *112*, E392–E401.
- (50) Janssen, R. H. H.; Vilà-Guerau de Arellano, J.; Ganzeveld, L. N.; Kabat, P.; Jimenez, J. L.; Farmer, D. K.; van Heerwaarden, C. C.; Mammarella, I. Combined effects of surface conditions, boundary layer dynamics and chemistry on diurnal SOA evolution. *Atmos. Chem. Phys.* **2012**, *12*, 6827–6843.
- (51) Shilling, J. E.; Chen, Q.; King, S. M.; Rosenoern, T.; Kroll, J. H.; Worsnop, D. R.; McKinney, K. A.; Martin, S. T. Particle mass yield in secondary organic aerosol formed by the dark ozonolysis of α -pinene. *Atmos. Chem. Phys.* **2008**, *8*, 2073–2088.
- (52) Pathak, R. K.; Stanier, C. O.; Donahue, N. M.; Pandis, S. N. Ozonolysis of α -pinene at atmospherically relevant concentrations: Temperature dependence of aerosol mass fractions (yields). *J. Geophys. Res.* **2007**, *112*, D03201.
- (53) Peeters, J.; Müller, J. J.-F.; Stavrakou, T.; Nguyen, V. S. V. Hydroxyl Radical Recycling in Isoprene Oxidation Driven by Hydrogen Bonding and Hydrogen Tunneling: the Upgraded LIM1Mechanism. *J. Phys. Chem. A* **2014**, *118*, 8625–8643.
- (54) Crounse, J. D.; Paulot, F.; Kjaergaard, H. G.; Wennberg, P. O. Peroxy radical isomerization in the oxidation of isoprene. *Phys. Chem. Phys.* **2011**, *13*, 13607–13613.
- (55) Riipinen, I.; Pierce, J. R.; Yli-Juuti, T.; Nieminen, T.; Häkkinen, S.; Ehn, M.; Junninen, H.; Lehtipalo, K.; Petäjä, T.; Slowik, J.; et al. Organic condensation: a vital link connecting aerosol formation to cloud condensation nuclei (CCN) concentrations. *Atmos. Chem. Phys.* **2011**, *11*, 3865–3878.
- (56) Wong, J. P. S.; Zhou, S.; Abbatt, J. P. D. Changes in Secondary Organic Aerosol Composition and Mass due to Photolysis: Relative Humidity Dependence. *J. Phys. Chem. A* **2015**, *119*, 4309–4316.
- (57) Hodzic, A.; Madronich, S.; Kasibhatla, P. S.; Tyndall, G.; Aumont, B.; Jimenez, J. L.; Lee-Taylor, J.; Orlando, J. Organic photolysis reactions in tropospheric aerosols: effect on secondary organic aerosol formation and lifetime. *Atmos. Chem. Phys. Discuss.* **2015**, *15*, 8113–8149.